

Measurement of Absolute Hadronic Branching Fractions of D_s Mesons*

N. E. Adam,¹ J. P. Alexander,¹ K. Berkelman,¹ D. G. Cassel,¹ J. E. Duboscq,¹
 K. M. Ecklund,¹ R. Ehrlich,¹ L. Fields,¹ L. Gibbons,¹ R. Gray,¹ S. W. Gray,¹
 D. L. Hartill,¹ B. K. Heltsley,¹ D. Hertz,¹ C. D. Jones,¹ J. Kandaswamy,¹ D. L. Kreinick,¹
 V. E. Kuznetsov,¹ H. Mahlke-Krüger,¹ P. U. E. Onyisi,¹ J. R. Patterson,¹ D. Peterson,¹
 J. Pivarski,¹ D. Riley,¹ A. Ryd,¹ A. J. Sadoff,¹ H. Schwarthoff,¹ X. Shi,¹ S. Stroiney,¹
 W. M. Sun,¹ T. Wilksen,¹ M. Weinberger,¹ S. B. Athar,² R. Patel,² V. Potlia,² J. Yelton,²
 P. Rubin,³ C. Cawfield,⁴ B. I. Eisenstein,⁴ I. Karliner,⁴ D. Kim,⁴ N. Lowrey,⁴ P. Naik,⁴
 C. Sedlack,⁴ M. Selen,⁴ E. J. White,⁴ J. Wiss,⁴ M. R. Shepherd,⁵ D. Besson,⁶
 T. K. Pedlar,⁷ D. Cronin-Hennessy,⁸ K. Y. Gao,⁸ D. T. Gong,⁸ J. Hietala,⁸ Y. Kubota,⁸
 T. Klein,⁸ B. W. Lang,⁸ R. Poling,⁸ A. W. Scott,⁸ A. Smith,⁸ P. Zweber,⁸ S. Dobbs,⁹
 Z. Metreveli,⁹ K. K. Seth,⁹ A. Tomaradze,⁹ J. Ernst,¹⁰ H. Severini,¹¹ S. A. Dytman,¹²
 W. Love,¹² V. Savinov,¹² O. Aquines,¹³ Z. Li,¹³ A. Lopez,¹³ S. Mehrabyan,¹³ H. Mendez,¹³
 J. Ramirez,¹³ G. S. Huang,¹⁴ D. H. Miller,¹⁴ V. Pavlunin,¹⁴ B. Sanghi,¹⁴ I. P. J. Shipsey,¹⁴
 B. Xin,¹⁴ G. S. Adams,¹⁵ M. Anderson,¹⁵ J. P. Cummings,¹⁵ I. Danko,¹⁵ J. Napolitano,¹⁵
 Q. He,¹⁶ J. Insler,¹⁶ H. Muramatsu,¹⁶ C. S. Park,¹⁶ E. H. Thorndike,¹⁶ F. Yang,¹⁶
 T. E. Coan,¹⁷ Y. S. Gao,¹⁷ F. Liu,¹⁷ M. Artuso,¹⁸ S. Blusk,¹⁸ J. Butt,¹⁸ J. Li,¹⁸ N. Mena,¹⁸
 R. Mountain,¹⁸ S. Nisar,¹⁸ K. Randrianarivony,¹⁸ R. Redjimi,¹⁸ R. Sia,¹⁸ T. Skwarnicki,¹⁸
 S. Stone,¹⁸ J. C. Wang,¹⁸ K. Zhang,¹⁸ S. E. Csorna,¹⁹ G. Bonvicini,²⁰ D. Cinabro,²⁰
 M. Dubrovin,²⁰ A. Lincoln,²⁰ D. M. Asner,²¹ K. W. Edwards,²¹ R. A. Briere,²² I. Brock,²²
 J. Chen,²² T. Ferguson,²² G. Tatishvili,²² H. Vogel,²² M. E. Watkins,²² and J. L. Rosner²³

(CLEO Collaboration)

¹*Cornell University, Ithaca, New York 14853*

²*University of Florida, Gainesville, Florida 32611*

³*George Mason University, Fairfax, Virginia 22030*

⁴*University of Illinois, Urbana-Champaign, Illinois 61801*

⁵*Indiana University, Bloomington, Indiana 47405*

⁶*University of Kansas, Lawrence, Kansas 66045*

⁷*Luther College, Decorah, Iowa 52101*

⁸*University of Minnesota, Minneapolis, Minnesota 55455*

⁹*Northwestern University, Evanston, Illinois 60208*

¹⁰*State University of New York at Albany, Albany, New York 12222*

¹¹*University of Oklahoma, Norman, Oklahoma 73019*

¹²*University of Pittsburgh, Pittsburgh, Pennsylvania 15260*

¹³*University of Puerto Rico, Mayaguez, Puerto Rico 00681*

¹⁴*Purdue University, West Lafayette, Indiana 47907*

¹⁵*Rensselaer Polytechnic Institute, Troy, New York 12180*

¹⁶*University of Rochester, Rochester, New York 14627*

¹⁷*Southern Methodist University, Dallas, Texas 75275*

¹⁸*Syracuse University, Syracuse, New York 13244*

¹⁹*Vanderbilt University, Nashville, Tennessee 37235*

²⁰*Wayne State University, Detroit, Michigan 48202*

²¹*Carleton University, Ottawa, Ontario, Canada K1S 5B6*

²²*Carnegie Mellon University, Pittsburgh, Pennsylvania 15213*
²³*Enrico Fermi Institute, University of Chicago, Chicago, Illinois 60637*
(Dated: 24 July 2006)

Abstract

We report preliminary measurements of absolute hadronic branching fractions of D_s mesons determined using a double tag technique. These measurements are from 195 pb^{-1} of e^+e^- collisions recorded at center of mass energies near 4.17 GeV with the CLEO-c detector at CESR. We obtain absolute branching fractions for D_s^+ decays to $K_S^0 K^+$, $K^- K^+ \pi^+$, $K^- K^+ \pi^+ \pi^0$, $\pi^+ \pi^+ \pi^-$, $\pi^+ \eta$, and $\pi^+ \eta'$. We discuss the problems inherent in measuring accurately the branching fraction for $D_s^+ \rightarrow \phi \pi^+$, which is often used as a reference mode for measurement of other D_s^+ branching fractions, and provide a measurement of a branching fraction that may be useful for this purpose.

*Submitted to the 33rd International Conference on High Energy Physics, July 26 - August 2, 2006, Moscow

I. INTRODUCTION

Absolute measurements of hadronic charm meson branching fractions play a central role in the study of the weak interaction because they serve to normalize many important B and D meson branching fractions. The importance of many of these branching fractions is enhanced by their roles in determining elements of the Cabibbo-Kobayashi-Maskawa (CKM) matrix [1].

Absolute D_s^1 branching fractions have not been measured as accurately as those for D^+ and D^0 [2], due to difficulties in determining the total number of D_s mesons produced in an experiment. The current best measurements of $\mathcal{B}(D_s^+ \rightarrow \phi\pi^+)$, which is usually used to normalize measurements of other D_s decay modes, are CLEO and BaBar results obtained using $B^0 \rightarrow D^{*-}D_s^{*+}$ events and a missing mass technique to extract the number of D_s^+ [3, 4].

In this contribution we describe measurements of absolute D_s branching fractions using a double tag technique. This technique was pioneered by the MARK-III Collaboration [5, 6] and more recently exploited in our precision measurements of absolute D^+ and D^0 branching fractions [7]. This technique relies on the fact that charm or strange quarks are always produced with the corresponding antiquark ($c\bar{c}$ or $s\bar{s}$) in e^+e^- annihilation. Hence, below the thresholds for $D_s^+D^-\bar{K}^0$ and $D_s^+\bar{D}^0K^-$ near $E_{cm} = 4.33$ GeV, production of a D_s^+ is always associated with production of a D_s^- , so observation of a D_s^\pm can serve as a tag for production of a D_s^\mp . In this experiment, data were accumulated near $E_{cm} = 4.17$ GeV (below the threshold for $D_s^{*\pm}D_s^{*\mp}$ production) where the production of $D_s^+D_s^-$ pairs is dominated by $e^+e^- \rightarrow D_s^{*\pm}D_s^{*\mp}$ [8] with the subsequent decays $D_s^{*\pm} \rightarrow D_s^\pm\gamma$ or $D_s^\pm\pi^0$.

Following the MARK III Collaboration, events in which either a D_s^+ or D_s^- is reconstructed without reference to the other particle are called single tag (ST) events, while events in which both the D_s^+ and D_s^- are reconstructed are called double tag (DT) events. Absolute branching fractions can then be determined from the ratios of DT events to ST events. If CP violation is negligible, then the branching fractions \mathcal{B}_j and $\mathcal{B}_{\bar{j}}$ for $D_s^+ \rightarrow j$ and $D_s^- \rightarrow \bar{j}$ are equal. However, the efficiencies ϵ_i and $\epsilon_{\bar{j}}$ for detection of these modes may be somewhat different since the cross sections for scattering of particles on nuclei may depend on the signs of the particles. With the assumption that $\mathcal{B}_j = \mathcal{B}_{\bar{j}}$, the numbers N_i and $N_{\bar{j}}$ of $D_s^+ \rightarrow i$ and $D_s^- \rightarrow \bar{j}$ ST events will be,

$$N_i = N_{D_s^*D_s} \mathcal{B}_i \epsilon_i \quad \text{and} \quad N_{\bar{j}} = N_{D_s^*D_s} \mathcal{B}_j \epsilon_{\bar{j}},$$

where $N_{D_s^*D_s}$ is the number of $D_s^{*\pm}D_s^{*\mp}$ events produced in the experiment. Then, the number of DT events with $D_s^+ \rightarrow i$ and $D_s^- \rightarrow \bar{j}$ will be,

$$N_{i\bar{j}} = N_{D_s^*D_s} \mathcal{B}_i \mathcal{B}_j \epsilon_{i\bar{j}},$$

where $\epsilon_{i\bar{j}}$ is the efficiency for detecting the DT. Hence, the ratio of DT events ($N_{i\bar{j}}$) to ST events ($N_{\bar{j}}$) provides an absolute measurement of the branching fraction \mathcal{B}_i ,

$$\mathcal{B}_i = \frac{N_{i\bar{j}} \epsilon_{\bar{j}}}{N_{\bar{j}} \epsilon_{i\bar{j}}}.$$

¹ Generally D_s will refer to either D_s^+ or D_s^- , and specification of an explicit D_s^\pm state and its decay daughters will imply a corresponding relationship for the D_s^\mp and its daughters.

Note that $\epsilon_{i\bar{j}} \approx \epsilon_i \epsilon_{\bar{j}}$, so many systematic uncertainties nearly cancel in the ratio $\epsilon_{\bar{j}}/\epsilon_{i\bar{j}}$, and a branching fraction \mathcal{B}_i obtained using this procedure is nearly independent of the efficiency of the tagging mode. Of course, \mathcal{B}_i is sensitive to ϵ_i and its uncertainties. Finally, the number of $D_s^+ D_s^-$ pairs that were produced is given by,

$$N_{D_s^+ D_s^-} = \frac{N_i N_{\bar{j}}}{N_{i\bar{j}}} \frac{\epsilon_{i\bar{j}}}{\epsilon_i \epsilon_{\bar{j}}}.$$

We studied six decay modes, $D_s^+ \rightarrow K_S^0 K^+$, $D_s^+ \rightarrow K^- K^+ \pi^+$, $D_s^+ \rightarrow K^- K^+ \pi^+ \pi^0$, $D_s^+ \rightarrow \pi^+ \pi^+ \pi^-$, $D_s^+ \rightarrow \pi^+ \eta$, and $D_s^+ \rightarrow \pi^+ \eta'$, and their charge conjugates in this analysis. For each mode we report the average of the branching fractions for D_s^+ and D_s^- . We detected neutral kaon candidates in the $K_S^0 \rightarrow \pi^+ \pi^-$ mode, η candidates in the $\eta \rightarrow \gamma\gamma$ mode, and η' candidates in the $\eta' \rightarrow \pi^+ \pi^- \eta$ mode.

II. THE CLEO DETECTOR AND PARTICLE SELECTION

The CLEO-c detector is a modification of the CLEO III detector [9–11], in which the silicon-strip vertex detector was replaced with a six-layer vertex drift chamber, whose wires are all at small stereo angles to the chamber axis [12]. The charged particle tracking system, consisting of this vertex drift chamber and a 47-layer central drift chamber [10] operates in a 1.0 T magnetic field, oriented along the beam axis. The momentum resolution of the tracking system is approximately 0.6% at $p = 1$ GeV/ c . Photons are detected in an electromagnetic calorimeter, composed of 7800 CsI(Tl) crystals [9], which attains a photon energy resolution of 2.2% at $E_\gamma = 1$ GeV and 5% at 100 MeV. The solid angle coverage for charged and neutral particles of the CLEO-c detector is 93% of 4π . We utilize two particle identification (PID) devices to separate K^\pm from π^\pm : the central drift chamber, which provides measurements of ionization energy loss (dE/dx), and, surrounding this drift chamber, a cylindrical ring-imaging Cherenkov (RICH) detector [11], whose active solid angle is 80% of 4π . The combined dE/dx -RICH PID system has a pion or kaon efficiency $> 90\%$ and a probability of pions faking kaons (or vice versa) $< 5\%$.

The response of the detector is studied with a detailed GEANT-based [13] Monte Carlo (MC) simulation of the CLEO detector for particle trajectories generated by EvtGen [14] and final state radiation (FSR) predicted by PHOTOS [15]. Simulated events are processed in a fashion similar to data. The integrated luminosity (\mathcal{L}) of the data sample is measured using e^+e^- Bhabha events in the calorimeter [16], where the event count normalization is provided by the detector simulation.

Charged tracks are required to be well-measured and to satisfy criteria based on the track fit quality. They must also be consistent with coming from the interaction point in three dimensions. Pions and kaons are identified by consistency with the expected dE/dx and RICH information, when available. We select K_S^0 candidates from pairs of oppositely-charged tracks that are constrained to a vertex, and that have $|M(\pi^+ \pi^-) - M_{K^0}| < 6.3$ MeV/ c^2 , where M_{K^0} [2] is the known K_S^0 mass. The 6.3 MeV/ c^2 limit is approximately 3σ .

We form π^0 (η) candidates from photon pairs with invariant mass within 3 standard deviations (σ) of the known π^0 (η) mass, M_{π^0} (M_η) [2], where $\sigma \approx 5$ –7 MeV/ c^2 depending on photon energy and location. These candidates are then fit kinematically with their masses constrained to M_{π^0} (M_η). We reconstruct η' candidates in the decay more $\eta' \rightarrow \pi^+ \pi^- \eta$ and require $0.9478 < M(\eta') < 0.9678$ GeV/ c^2 .

III. DATA SAMPLE AND CANDIDATE SELECTION

The data sample for this measurement consists of 179 pb⁻¹ collected at $E_{cm} = 4.17$ GeV, 10 pb⁻¹ collected at $E_{cm} = 4.16$ GeV, and 6 pb⁻¹ collected at $E_{cm} = 4.18$ GeV. We collected the 4.16 GeV data and 4.18 GeV data in a scan of center-of-mass energies designed to determine the optimal energy for studying D_s decays [8].

Most of the D_s mesons at E_{cm} near 4.17 GeV come from $D_s^{*\pm}D_s^\mp$ events, and we impose kinematic cuts on the D_s candidates to require this topology. In such events, $D_s^{*\pm} \rightarrow D_s^\pm\gamma$ or $D_s^\pm\pi^0$, so one of the D_s is produced directly and the other is a secondary from D_s^* decay. We use two variables to select D_s decay candidates and isolate signals from backgrounds. One variable is the candidate invariant mass,

$$M(D_s)c^2 = \sqrt{E(D_s)^2 - \mathbf{p}(D_s)^2c^2}, \quad (1)$$

where $\mathbf{p}(D_s)$ and $E(D_s)$ are the total momentum and energy, respectively, of the daughters of the candidate D_s . The particle energies are computed from particle momenta using the masses determined by PID. The other variable is the beam constrained mass,

$$M_{bc}c^2 \equiv \sqrt{E_0^2 - \mathbf{p}(D_s)^2c^2} \quad (2)$$

obtained by substituting the beam energy E_0 for the energy $E(D_s)$ of the candidate. We make the following observations and choices based on these observations for this analysis:

- We do not require full reconstruction of the event; *i.e.*, we make no attempt to find the γ or π^0 resulting from the D_s^* decay. This avoids a large efficiency loss and avoids substantial contributions to systematic errors that would arise from soft photon detection and which would affect ST and DT yields differently.
- The value of E_{cm} determines the momenta of the D_s and D_s^* , so the momentum of the direct D_s is tightly constrained, and the momentum of the D_s from D_s^* decay has a somewhat wider distribution about the same value.
- The M_{bc} distribution of direct D_s mesons has a peak about 0.010 GeV/ c^2 wide centered at 2.04 GeV/ c^2 – somewhat above $M_{D_s} = 1.9683$ GeV/ c^2 [2]. The M_{bc} distribution of the D_s daughters from D_s^* decay is broader and relatively flat from about 2.015 GeV/ c^2 to about 2.065 GeV/ c^2 . These two components of the M_{bc} mass distribution are clearly evident in Fig. 1. The upper limit of the M_{bc} distribution is just the beam energy E_0 , while the lower limit is determined by the maximum momentum of the secondary D_s candidates.
- In our selection of D_s candidates, we use M_{bc} as a proxy for this momentum, since it is insensitive to variations in E_{cm} and allows easy integration of data taken at different energies.
- We use the invariant mass $M(D_s)$ of the D_s candidate as our primary analysis variable. It has very little correlation with M_{bc} in the region of interest.

We require $|M(D_s) - M_{D_s}| < 0.085$ GeV/ c^2 and a “loose” cut $M_{bc} > 2.01$ GeV/ c^2 , for D_s candidates in all decay modes. For the $D_s^+ \rightarrow K^-K^+\pi^+\pi^0$ and $D_s^+ \rightarrow \pi^+\pi^+\pi^-$ modes, we require additional “tight” cuts of $M_{bc} > 2.034$ GeV/ c^2 and $M_{bc} > 2.035$ GeV/ c^2 , respectively. The loose cut includes the entire range of M_{bc} resulting in maximum efficiency. The tight cut selects all of the directly-produced D_s and over half of the indirect D_s as well. This reduces the background while reducing the impact of initial-state radiation smearing of efficiency.

Furthermore, for ST candidates we require:

- $D_s^+ \rightarrow K_s^0 K^+$: We reject candidates with $M(K^+\pi^-) > 1.83 \text{ GeV}/c^2$ to eliminate a small background from $\bar{D}^0 \rightarrow K^+\pi^-$ decays.
- $D_s^+ \rightarrow K^- K^+\pi^+$: We reject candidates with $1.845 < M(K^-K^+) < 1.88 \text{ GeV}/c^2$ to eliminate a small background from $D^0 \rightarrow K^-K^+$ decays.
- $D_s^+ \rightarrow K^- K^+\pi^+\pi^0$: We require $\mathbf{p}_{\pi^0} > 0.1 \text{ GeV}/c$ to reduce a background from $D^{*\pm}$ and D^{*0} decays, and we reject candidates with $1.86 < M(K^-K^+\pi^+) < 1.88 \text{ GeV}/c^2$ to eliminate a small background from $D^+ \rightarrow K^-K^+\pi^+$ decays.
- $D_s^+ \rightarrow \pi^+\pi^+\pi^-$: We reject candidates if either $\pi^+\pi^-$ candidate has $475 < M(\pi^+\pi^-) < 520 \text{ MeV}/c^2$ (to eliminate $K_s^0 \rightarrow \pi^+\pi^-$ decays), or either candidate has $1.840 < M(\pi^+\pi^-) < 1.885 \text{ GeV}/c^2$ (to eliminate $D^0 \rightarrow \pi^+\pi^-$ decays). Also, when the π^- is assumed to be a K^- and is assigned the K^- mass, we reject the D_s^+ candidate if either $K^-\pi^+$ combination had $1.845 < M(K^-\pi^+) < 1.880 \text{ GeV}/c^2$ to eliminate background from $D^0 \rightarrow K^-\pi^+$.
- In every event, for each mode and each charge, we choose the best ST candidate. We accept the candidate with the smallest value of $|M_{bc} - \widehat{M}|$, where $\widehat{M} = 2.040553 \text{ GeV}/c^2$ is the value at which M_{bc} peaks for daughters of direct D_s decays. An event can have candidates in more than one mode for a given D_s charge.

Furthermore, for DT candidates we require:

- In a DT event, one of the D_s will be direct and the other will be the daughter of a D_s^* decay. We impose the loose M_{bc} requirement on both of the D_s candidates.
- Each of the D_s candidates in a DT event must pass the ST requirements described above.
- To resolve multiple candidates, we select the candidate with total invariant mass closest to $2M_{D_s}$. This variable is orthogonal to the difference between the masses of the two candidates, which is used in selecting signal and background sideband events as described below.

IV. EFFICIENCIES AND YIELDS

To develop our analysis procedures and estimate efficiencies, we simulated two types of D_s meson decays:

- “signal” decays in which a D_s^+ or D_s^- decays in one of the 6 modes measured in this analysis, and
- “generic” decays in which a D_s^+ or D_s^- decays in a manner consistent with the decay modes and branching fractions in the PDG compilation [2], extended with additional decays that are expected to be present.

Using these two types of simulated decays, we generated three types of Monte Carlo (MC) events:

- generic Monte Carlo events, in which both the D_s^+ and the D_s^- decay generically,
- single tag signal Monte Carlo events, in which either the D_s^+ or the D_s^- always decays in one of the 6 modes measured in this analysis while the D_s^- or D_s^+ , respectively, decays generically, and
- double tag signal Monte Carlo events, in which both the D_s^+ and the D_s^- decay in one of the 6 modes in this analysis.

In these events, both the D_s^+ and D_s^- have a 50% probability of being produced from a $D_s^{\pm*}$.

We also generated MC samples of continuum u , d , s quark production and production of non-strange charmed meson states, which form the major background to this analysis. The relative production rates are set by information obtained from the scan of this energy region [8].

We obtained the ST efficiencies and yields by fitting $M(D_s)$ distribution for each mode in single tag MC events. The fit functions and their parameters, as well as efficiencies were determined from $M(D_s)$ distributions from signal Monte Carlo simulations.

The ST distributions are fit with a linear backgrounds and a signal lineshapes. Two Gaussian distributions were chosen for the lineshapes for the $K_S^0 K^+$, $K^- K^+ \pi^+$, $\pi^+ \pi^+ \pi^-$, and $\pi^+ \eta'$ modes. The lineshapes chosen for $K^- K^+ \pi^+ \pi^0$ and $\pi^+ \eta$ decays was the sum of a narrow Gaussian and a wider Crystal Ball function [17], whose low mass tail simulates energy leakage in the CsI calorimeter. The lineshape parameters are fixed separately for each charge from candidates that are matched to the generator-level D_s . The ST efficiencies obtained from signal MC events are given in Table I. The fits to $M(D_s)$ distributions in data are illustrated in Figs. 2–7, and the corresponding yields from data are given in Table II.

TABLE I: Single tag efficiencies (in %) obtained from signal MC events. Sec. VI describes small corrections that must be applied to these efficiencies.

D_s^+ Mode	D_s^+	D_s^-
$K_S K^+$	37.58 ± 0.24	37.43 ± 0.24
$K^- K^+ \pi^+$	44.79 ± 0.25	43.90 ± 0.25
$K^- K^+ \pi^+ \pi^0$	12.32 ± 0.19	12.69 ± 0.19
$\pi^+ \pi^+ \pi^-$	49.52 ± 0.26	49.36 ± 0.26
$\pi^+ \eta$	19.99 ± 0.21	19.09 ± 0.21
$\pi^+ \eta'$	5.29 ± 0.12	5.53 ± 0.12

TABLE II: Single tag yields obtained from fits to the $M(D_s)$ distributions of data.

	$K_S K^+$	$K^- K^+ \pi^+$	$K^- K^+ \pi^+ \pi^0$	$\pi^+ \pi^+ \pi^-$	$\pi^+ \eta$	$\pi^+ \eta'$
D_s^+	1055.0 ± 39.4	4319.1 ± 88.8	1342.3 ± 101.9	969.5 ± 79.3	547.0 ± 49.6	361.8 ± 23.4
D_s^-	927.6 ± 37.3	4352.2 ± 88.7	1371.9 ± 102.9	946.7 ± 77.6	570.0 ± 49.8	371.5 ± 23.6

We obtain double tag yields by counting the numbers of events in signal regions in $M(D_s^-)$ vs $M(D_s^+)$ planes and subtracting the numbers of events in sideband regions of the corresponding planes. We find that combinatoric backgrounds from D^+ , D^0 , and continuum events tend to be distributed along lines of constant total mass, $M_T \equiv M(D_s^+) + M(D_s^-)$. Both signal and sideband regions use subsets of the M_T region, $3.915 < M_T < 3.960$ GeV/ c^2 . Within this M_T region, the signal region is $|\Delta M| < 30$ MeV/ c^2 , while the sideband regions are $50 < |\Delta M| < 150$ MeV/ c^2 , where $\Delta M = M(D_s^+) - M(D_s^-)$. We see no evidence for any background to peak in the signal region, so we are confident that the events in these

sideband regions provide reasonable estimates of the backgrounds in the signal regions. DT efficiencies obtained from signal MC events are given in Table III and DT yields obtained from data are given in Table IV.

TABLE III: Double tag efficiencies (in %) obtained from signal MC events. Sec. VI describes small corrections that must be applied to these efficiencies.

	$K_S K^-$	$K^+ K^- \pi^-$	$K^+ K^- \pi^- \pi^0$	$\pi^- \pi^- \pi^+$	$\pi^- \eta$	$\pi^- \eta'$
$K_S K^+$	14.02 ± 0.17	17.30 ± 0.19	6.74 ± 0.13	22.84 ± 0.21	6.64 ± 0.12	1.96 ± 0.07
$K^- K^+ \pi^+$	16.75 ± 0.19	20.35 ± 0.20	7.65 ± 0.13	27.91 ± 0.22	8.01 ± 0.14	2.39 ± 0.08
$K^- K^+ \pi^+ \pi^0$	6.74 ± 0.13	7.88 ± 0.13	2.40 ± 0.08	11.09 ± 0.16	3.17 ± 0.09	1.00 ± 0.05
$\pi^+ \pi^+ \pi^-$	22.48 ± 0.21	27.69 ± 0.22	11.22 ± 0.16	35.94 ± 0.24	10.91 ± 0.16	3.17 ± 0.09
$\pi^+ \eta$	6.68 ± 0.12	8.34 ± 0.14	3.21 ± 0.09	10.88 ± 0.16	3.18 ± 0.09	0.92 ± 0.05
$\pi^+ \eta'$	1.94 ± 0.07	2.47 ± 0.08	0.94 ± 0.05	3.32 ± 0.09	0.92 ± 0.05	0.32 ± 0.03

V. BRANCHING FRACTIONS

We are unable to use the standard branching fraction fitter [18] created for our analysis of D^+ and D^0 branching fractions [7]. This fitter uses χ^2 minimization, which is not appropriate for the small yields and backgrounds in the DT modes. For this analysis, we have developed a binned-likelihood hybrid fitter which utilizes Gaussian statistics for the ST modes and Poisson statistics for the DT modes. The likelihood is maximized with the number of $D_s^{*\pm} D_s^\mp$ mesons ($N_{D_s^* D_s}$) and the branching fractions for the individual modes (\mathcal{B}_i) averaged over D_s^+ and D_s^- as the free parameters. The hybrid fitter treats properly the correlated systematic errors among quantities affecting ST efficiencies only. However, unlike the standard fitter, this fitter does not handle correlated systematic errors in efficiencies among double tag modes or between single tag modes and double tag modes. On the other hand, the approximate cancellation of systematic errors between DT and ST efficiencies is still utilized in computing overall systematic errors.

TABLE IV: Double tag yields obtained from data by subtracting backgrounds estimated from sidebands.

	$K_S K^-$	$K^+ K^- \pi^-$	$K^+ K^- \pi^- \pi^0$	$\pi^- \pi^- \pi^+$	$\pi^- \eta$	$\pi^- \eta'$
$K_S K^+$	7.7	27.0	18.7	7.3	4.0	5.0
$K^- K^+ \pi^+$	18.0	104.7	43.7	30.7	12.0	8.0
$K^- K^+ \pi^+ \pi^0$	8.7	35.7	14.0	13.3	1.0	5.7
$\pi^+ \pi^+ \pi^-$	3.3	22.7	16.0	13.3	4.7	4.0
$\pi^+ \eta$	0.0	10.0	2.7	6.0	1.0	1.7
$\pi^+ \eta'$	3.0	10.0	3.0	3.7	1.0	0.0

We tested this hybrid fitter extensively in MC simulations and with data from our D^+ and D^0 analysis. This fitter produces results very close to the standard fitter in that analysis. We also tested this hybrid fitter with toy MC samples with ST and DT yields comparable to those in this analysis. We find that the hybrid fitter shows less bias and produces pull distributions that are more nearly Gaussian and with standard deviations closer to 1.

The branching fractions and statistical errors resulting from applying the hybrid fitter to the ST and DT yields are given in Table V. The table also includes the systematic errors described in the next section.

TABLE V: Branching fractions obtained from the ST and DT yields, using the hybrid fitter. The errors are statistical and systematic, respectively.

D_s^+ Mode	\mathcal{B} (%)
$K_S K^+$	$1.50 \pm 0.09 \pm 0.05$
$K^- K^+ \pi^+$	$5.57 \pm 0.30 \pm 0.19$
$K^- K^+ \pi^+ \pi^0$	$5.62 \pm 0.33 \pm 0.51$
$\pi^+ \pi^+ \pi^-$	$1.12 \pm 0.08 \pm 0.05$
$\pi^+ \eta$	$1.47 \pm 0.12 \pm 0.14$
$\pi^+ \eta'$	$4.02 \pm 0.27 \pm 0.30$

VI. SYSTEMATIC ERRORS

A. Detector Simulation

Using a missing mass technique, we measure efficiencies for reconstructing tracks, K_S^0 decays, and π^0 decays in both data and simulated events. We fully reconstruct $\psi(3770) \rightarrow D\bar{D}$, $\psi(2S) \rightarrow J/\psi\pi^+\pi^-$, and $\psi(2S) \rightarrow J/\psi\pi^0\pi^0$ events, leaving out one particle, for which we wish to determine the efficiency. The missing mass of this combination peaks at the mass of the omitted particle, whether or not it is detected. Then, the desired efficiency is the fraction of this peak with this particle correctly reconstructed. We find good agreement between efficiencies in data and simulated events. The relative uncertainties in these determinations, 0.35% per charged particle track, 1.1% per K_S^0 , and 5.0% per π^0 or η . Extrapolation from the relatively low energies of the pions in $\psi(2S) \rightarrow J/\psi\pi^0\pi^0$ decay to the higher energies encountered in our D_s decay modes contributes significantly to the larger uncertainties for π^0 and η simulation.

B. Charged Particle Identification

We study the simulation of the PID efficiencies for charged pions and kaons using decays with unambiguous particle content, such as $D^0 \rightarrow K_S^0\pi^+\pi^-$ and $D^+ \rightarrow K^-\pi^+\pi^+$. We find small momentum dependent corrections to efficiencies for pions and kaons. The uncertainties in these corrections are estimated to be less than 0.2% for pions and 0.3% for kaons. We use these corrections to compute efficiency corrections which depend on the decay mode,

TABLE VI: Corrections to the efficiencies from signal MC simulations, for particle ID, resonant substructure, and their product. The ST efficiencies given in Table I are corrected by the product factors in this table, while the DT efficiencies given in Table III are corrected by the product factors for the two modes in the DT. The uncertainties are the contributions of these factors to the systematic error. The quoted uncertainties for the $K^-K^+\pi^+$ and $K^-K^+\pi^+\pi^0$ modes cover the ranges of corrections for the submodes.

Mode	PID	Resonant Substructure	Product
$K_S^0 K^+$	0.989 ± 0.003	1	0.989 ± 0.003
$K^- K^+ \pi^+$	0.971 ± 0.008	1.000 ± 0.015	0.971 ± 0.017
$K^- K^+ \pi^+ \pi^0$	0.961 ± 0.014	1.033 ± 0.060	0.993 ± 0.062
$\pi^+ \pi^+ \pi^-$	0.989 ± 0.006	1.000 ± 0.020	0.989 ± 0.021
$\pi^+ \eta$	0.998 ± 0.002	1	0.998 ± 0.002
$\pi^+ \eta'$	0.968 ± 0.006	1	0.968 ± 0.006

and on submodes for modes with multiple resonant states. The correction factors and their uncertainties are listed in Table VI. The quoted uncertainties for the $K^-K^+\pi^+$ and $K^-K^+\pi^+\pi^0$ modes cover the range of correction factors estimated for the submodes.

C. Resonant Substructure

The resonant substructures of the inclusive multibody modes in this analysis are poorly understood. Since final-state momenta and angular distributions are sensitive to the intermediate resonances in these decays, the efficiencies will depend on the resonant substructure. We estimate possible corrections to efficiencies and the associated systematic uncertainties by estimating the number of events in our data samples in the different resonant modes. We then estimate the range of possible corrections from the corrections for these different resonant modes. This correction does not apply to the two-body modes $K_S^0 K^+$, $\pi^+ \eta$, and $\pi^+ \eta'$. The estimated corrections to the efficiencies and the associated systematic uncertainties for the multibody modes are included in Table VI.

D. Single Tag Fitting Functions

To study possible differences between the MC lineshape and the lineshape in data, we perform two checks: We allow the overall mass and width of the signal lineshape to float (keeping the relative normalization and ratio of widths of the two Gaussians fixed), and we allow a quadratic term in the background. The maximum excursions of the yields of two additional fits from the yields of the normal fits are taken to be the systematic uncertainties. These excursions and the systematic uncertainties are included in Table VII.

TABLE VII: Systematic uncertainties due to uncertainties in the ST fitting functions. The middle two columns are yield excursions (averaged over charge) for using a quadratic background or allowing the $M(D_s)$ width and mass to float. The rightmost column is the systematic uncertainty assigned to single tag yields in this mode. All numbers are in percent (%).

Mode	Second-order Polynomial	Float Width & Mass	Systematic Uncertainty
$K_S^0 K^+$	-0.1	+0.1	± 0.1
$K^- K^+ \pi^+$	-0.5	+2.0	± 2.0
$K^- K^+ \pi^+ \pi^0$	+8.7	-10.8	± 10.8
$\pi^+ \pi^+ \pi^-$	+1.4	-2.1	± 2.1
$\pi^+ \eta$	-8.8	+11.1	± 11.1
$\pi^+ \eta'$	-4.8	+4.5	± 4.8

E. Initial State Radiation

Initial state radiation (ISR) can impact the M_{bc} requirement used in selection of decay modes by reducing the momenta of the D_s candidates, leading to high-side tails on the M_{bc} distributions for primary and secondary D_s mesons. By definition, M_{bc} is limited by the beam energy E_0

For the loose M_{bc} requirement, we accept all events from the lower kinematic limit to the beam energy (*i.e.* momenta from the upper kinematic limit to zero), so the cut is fully efficient regardless of ISR. The tight cuts used for the $K^+ K^- \pi^+ \pi^0$ and $\pi^+ \pi^+ \pi^-$ modes eliminate most of the lower half of the M_{bc} distribution for secondary D_s from D_s^* decay. Since the effect of ISR on the M_{bc} distribution is independent of decay mode, we study the comparison between MC and data using the high-statistics $D_s^+ \rightarrow K^+ K^- \pi^+$ mode. First, we compare loose and tight yields in data and MC simulation without ISR. We find $R_{Data} \equiv y_L/y_T = 0.807 \pm 0.008$, where y_L and y_T are the yields in data from the loose and tight cuts respectively. The corresponding number from MC simulation without ISR is $R_{T\overline{SR}} = 0.814 \pm 0.003$, so the two ratios agree within 1%. We then study this ratio in a MC simulation with ISR, and find $R_{ISR} = 0.806 \pm 0.005$, agreeing with the other two ratios within 1%. We do not correct for this effect, but we include a 1% systematic uncertainty in the ST efficiencies for the $K^+ K^- \pi^+ \pi^0$ and $\pi^+ \pi^+ \pi^-$ modes where we apply this tight M_{bc} cut.

F. Multiple Candidates

If there is more than one candidate for a given mode, and we select only one, there is some inefficiency associated with making the incorrect choice for this mode. This inefficiency is modeled in MC simulations, but if the multiple candidate rates are significantly different in data and MC simulations, there is likely to be an efficiency difference. We examine signal and sideband multiplicity distributions; the invariant mass regions for these two data samples are $1.955 < M(D_s) < 1.980$ GeV/ c^2 and $1.90 < M(D_s) < 1.93$ GeV/ c^2 , respectively. We compare multiplicity distributions for data and MC simulations after subtracting sideband

distributions from signal distributions. There is good agreement between data and MC multiplicity distributions, although data multiplicities are generally marginally larger.

If we assume we can do no better than randomly choose candidates (so, for example, the efficiency is down 50% for two candidates, 67% for three), we can limit the effect of this difference on the total efficiency. We find that this effect on ST efficiencies is negligible for the $K_S^0 K^+$, $K^+ K^- \pi^+$, and $\pi^+ \eta'$ modes. For the other three modes we assign systematic uncertainties to the ST efficiencies of: 3% for $K^+ K^- \pi^+ \pi^0$, 1% for $\pi^+ \pi^+ \pi^-$, and 0.5% for $\pi^+ \eta$.

G. Other Possible Systematic Uncertainties

Several potential systematic errors do not contribute significantly to the systematic uncertainties of these measurements.

We checked our analysis procedure, the internal consistency of our Monte Carlo simulations, and the utility of the hybrid fitter by analyzing a generic MC sample corresponding to approximately six times the luminosity of the current data sample. This sample included appropriately weighted samples of all open charm channels at 4.17 GeV. There is no significant evidence for bias in the analysis or fitting procedure, so we do not include a systematic error for our procedures.

Data were accumulated in three separate data sets; we do not observe significant variations of yields per unit luminosity over these data sets.

The ST yields for D_s^+ and D_s^- are consistent, so we do not include a contribution to the systematic error for the differences in efficiencies or yields for D_s^+ and D_s^- .

The D_s^+ daughters from the isospin violating decay $D_s^{*+} \rightarrow D_s^+ \pi^0$ have a different momentum distribution from those from $D_s^{*+} \rightarrow D_s^+ \gamma$ decay. The yields of the $K^+ K^- \pi^+ \pi^0$ and $\pi^+ \pi^+ \pi^-$ modes are sensitive to this momentum difference due to the tight M_{bc} requirements for these modes. However, the effect is small due to the small branching fraction for the $D_s^+ \pi^0$ mode. We estimate that the possible effect is of $\mathcal{O}(0.14\%)$ and we ignore it.

Potential differences in M_{bc} resolution in MC simulations and data can affect the efficiency for the tight cuts used for the $K^+ K^- \pi^+ \pi^0$ and $\pi^+ \pi^+ \pi^-$ modes. The M_{bc} resolution $\sigma_{M_{bc}}$ is dominated by the beam energy spread. If we vary this by 10%, we expect an efficiency change of $\mathcal{O}(0.2\%)$ or less.

Because we use invariant mass as our fit variable, the only backgrounds that we expect to peak in our signal regions of $M(D_s)$ are those that produce the same final state daughters. The Cabibbo suppressed decay $D_s^+ \rightarrow K_S^0 \pi^+$ can fake $D_s^+ \rightarrow \pi^+ \pi^+ \pi^-$ decays. As described above, we eliminate this background with cuts on the $\pi^+ \pi^-$ mass for either pair, so we do not include a correction or systematic error for this possible background. Via misidentification of the K^+ , the decay $D_s^+ \rightarrow K^+ \pi^+ \pi^-$ can fake the $K_S^0 \pi^+$ mode. We search for such a signal in data and find none, so we do not include a correction or systematic error for this potential background.

H. Summary of Systematic Errors

Table VIII summarizes the systematic uncertainties for the inclusive branching fractions measured in this analysis.

TABLE VIII: Summary of systematic uncertainties in efficiencies for inclusive branching fraction measurements. This list excludes systematics from MC statistics and fit function systematics obtained in the data fits. Where ranges are given, the values for individual modes can be found in Table VI for Particle Identification, Table VII for ST Fit Functions, and Sec. VI F for Multiple Candidate Rates.

Source	Uncertainty (%)	Affects
Detector Simulation	0.35	Tracks
	1.1	K_S^0
	5.0	π^0
	5.0	η
Particle Identification	0.3–1.4	Per mode
Resonant Substructure	1.5	$K^+K^-\pi^+$
	6.0	$K^-K^+\pi^+\pi^0$
	2.0	$\pi^+\pi^+\pi^-$
ST Fit Functions	0.1–11.1	Per mode
Initial State Radiation	1.0	$K^-K^+\pi^+\pi^0$
	1.0	$\pi^+\pi^+\pi^-$
Multiple Candidate Rates	0.0–3.0	Per mode

The systematic uncertainties discussed in this section were added in quadrature to obtain the systematic uncertainties given in Table V for the six inclusive modes included in this analysis.

VII. PARTIAL BRANCHING FRACTIONS FOR $D_s^+ \rightarrow K^-K^+\pi^+$

The decay $D_s^+ \rightarrow \phi\pi^+ \rightarrow K^-K^+\pi^+$, being one of the largest and easiest to reconstruct D_s decays, has historically been used as a reference mode. Many analyses take advantage of the small ϕ width and impose cuts on the K^-K^+ system in a $K^-K^+\pi^+$ event to enhance the signal significance, generally in the form of an invariant mass cut around the ϕ and possibly a helicity angle cut (to take advantage of the ϕ polarization). Our inclusive branching fraction results do not directly connect to analyses that select this submode for background suppression.

We have investigated the K^-K^+ invariant mass spectrum in $K^-K^+\pi^+$ decays. The mass distribution, obtained by fitting for the D_s signal in bins of $M(K^-K^+)$, is shown in Fig. 10. Intrinsic detector resolution on $M(K^-K^+)$ near the ϕ mass is about 1 MeV/ c^2 . We observe a clear peak arising from the $\phi\pi^+$ intermediate state. However there is a broad signal from another source, extending from K^-K^+ threshold to masses above M_ϕ . This signal is found to have kinematic distributions indicative of a scalar. The E687 collaboration has published [19] and the FOCUS collaboration has reported [20] Dalitz plot analyses of $D_s^+ \rightarrow K^-K^+\pi^+$ and find significant scalar contributions from $f_0(980)$ (or $a_0(980)$) in this mass region. Because of this extra signal, an exclusive $\phi\pi^+$ branching fraction is not necessarily useful for normalization purposes, and ignoring the scalar contribution leads to

TABLE IX: Efficiency, yields in data, and partial branching fraction results for two choices of $M(K^-K^+)$ cuts in $K^-K^+\pi^+$ events.

Branching Fraction	Efficiency (%)	Data Yield	Result (%)
\mathcal{B}_{10}	43.3 ± 1.3	$3062 \pm 58 \pm 11$	$1.98 \pm 0.12 \pm 0.09$
\mathcal{B}_{20}	43.4 ± 1.3	$3482 \pm 63 \pm 13$	$2.25 \pm 0.13 \pm 0.12$

the branching fraction being ill-defined by $\mathcal{O}(5\%)$ depending on the specific choice of cuts.

We report here measurements of the inclusive branching fraction for $K^-K^+\pi^+$ decays where the K^-K^+ system lies in specific mass ranges. We define

$$\mathcal{B}_{\Delta M} \equiv \mathcal{B}(D_s^+ \rightarrow K^-K^+\pi^+) \text{ for } |M(K^-K^+) - 1.0195 \text{ GeV}/c^2| < \Delta M \text{ MeV}/c^2$$

and measure \mathcal{B}_{10} and \mathcal{B}_{20} .

To measure these partial branching fractions we perform fits to $K^-K^+\pi^+$ signal events where $M(K^-K^+)$ passes the respective cuts to obtain yields $N_{\Delta M}$. The efficiencies $\epsilon_{\Delta M}$ for event reconstruction are obtained from signal MC samples of pure $\phi\pi^+$ and $f_0(980)\pi^+$ production. The uncertainty arises largely from differences in the reconstruction efficiencies for scalar and vector angular distributions. Uncertainties on the fit functions and detector resolution smearing of the mass distribution contribute 0.4% to the systematics on the yields for both branching fractions. We obtain the partial branching fractions from

$$\mathcal{B}_{\Delta M} = \frac{N_{\Delta M}}{2\epsilon_{\Delta M}N_{D_s^*D_s}}$$

utilizing the value of $N_{D_s^*D_s}$ we obtain in the fit to the six inclusive modes.

The efficiencies, data yields, and partial branching fraction results are shown in Table IX.

VIII. RESULTS AND CONCLUSIONS

We have reported preliminary absolute measurements of the branching fractions of D_s mesons to six final states, with total relative uncertainties ranging from 6.4% to 12.5%. We have also obtained measurements of two partial branching fractions, to $K^-K^+\pi^+$ substates with restricted values of $M(K^-K^+)$.

We gratefully acknowledge the effort of the CESR staff in providing us with excellent luminosity and running conditions. This work was supported by the National Science Foundation and the U.S. Department of Energy.

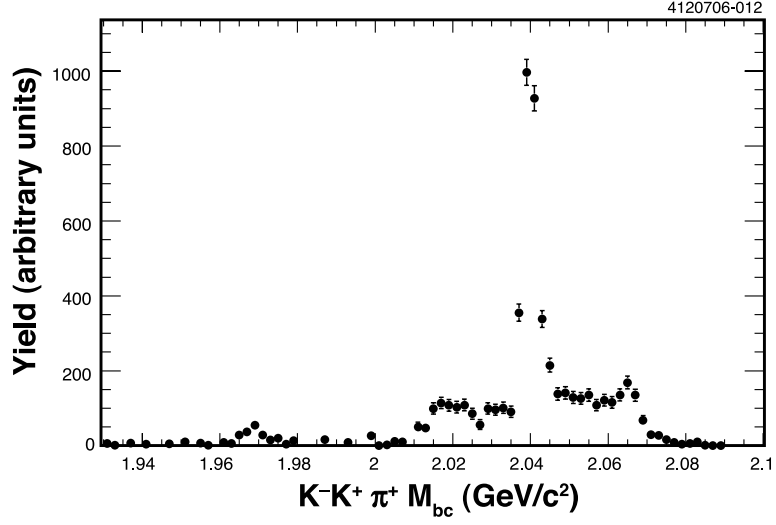


FIG. 1: M_{bc} distribution for $D_s^\pm \rightarrow K^- K^+ \pi^\pm$ events in data.

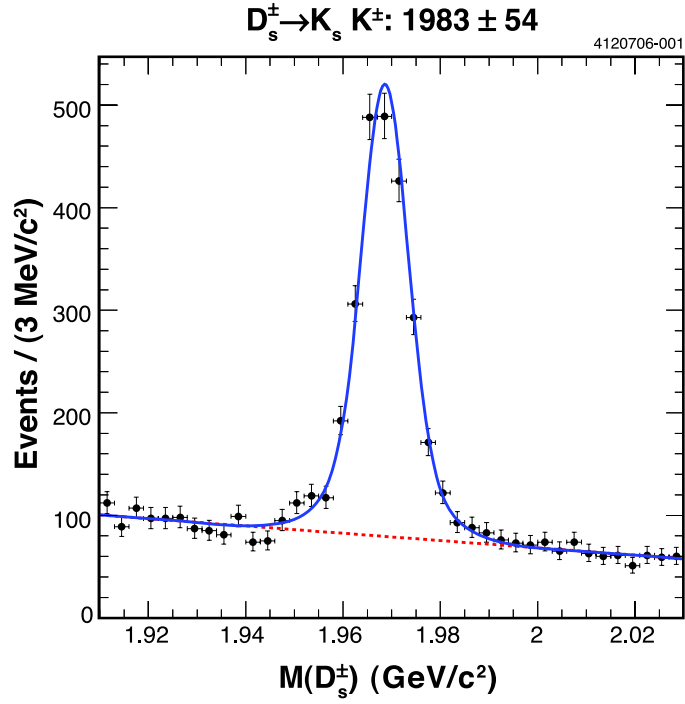


FIG. 2: Fits to single tag data for $D_s^\pm \rightarrow K_s^0 K^\pm$.

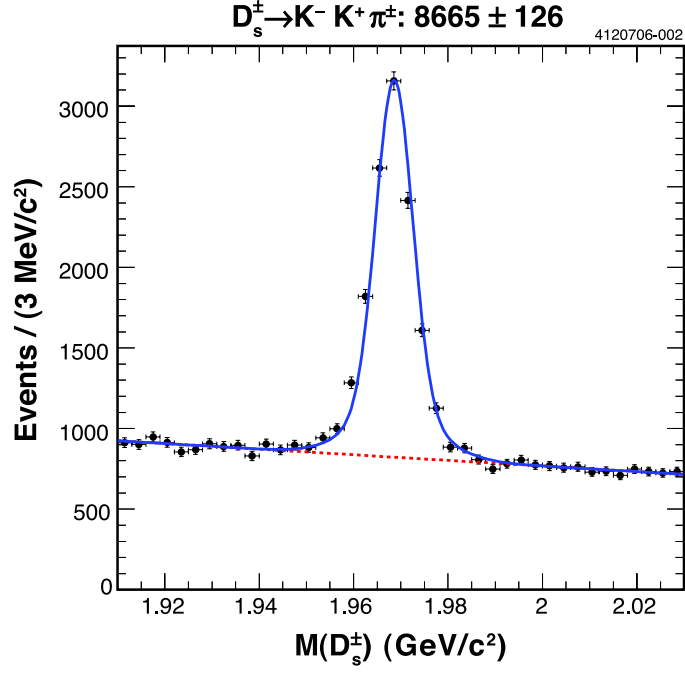


FIG. 3: Fits to single tag data for $D_s^\pm \rightarrow K^- K^+ \pi^\pm$.

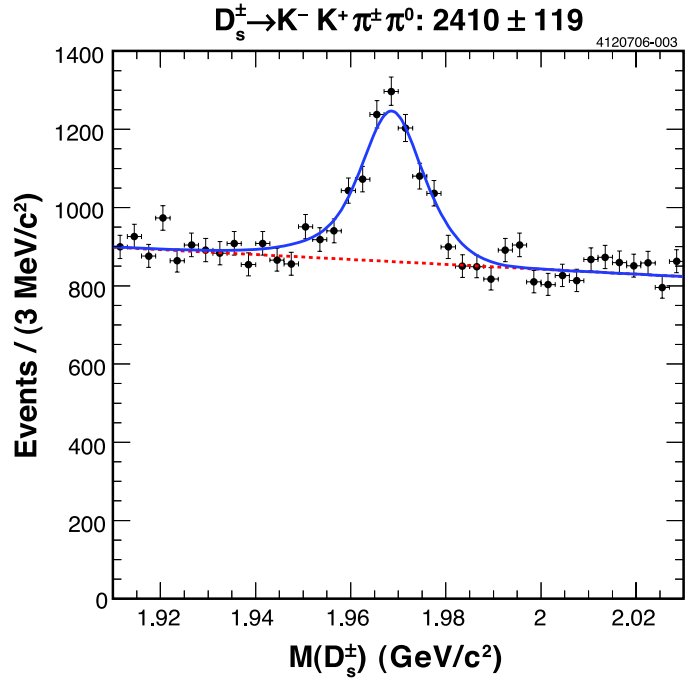


FIG. 4: Fits to single tag data for $D_s^\pm \rightarrow K^- K^+ \pi^\pm \pi^0$.

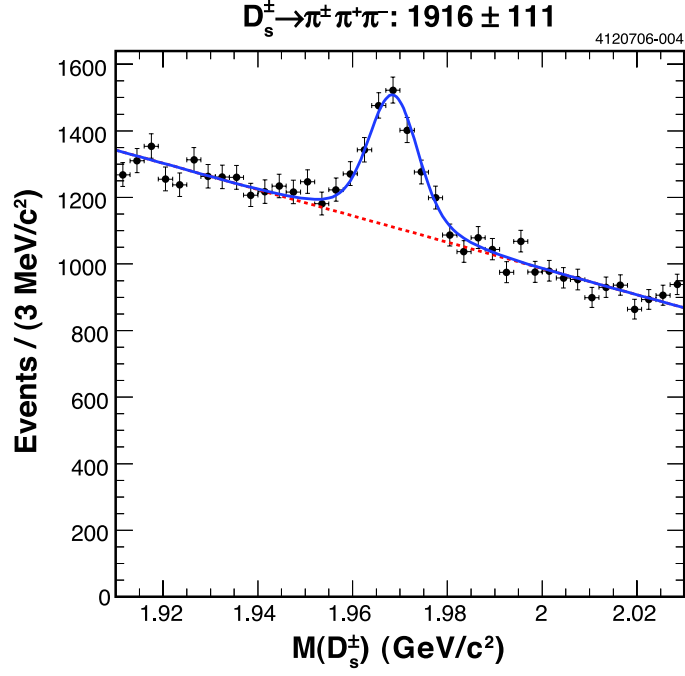


FIG. 5: Fits to single tag data for $D_s^\pm \rightarrow \pi^+ \pi^- \pi^\pm$.

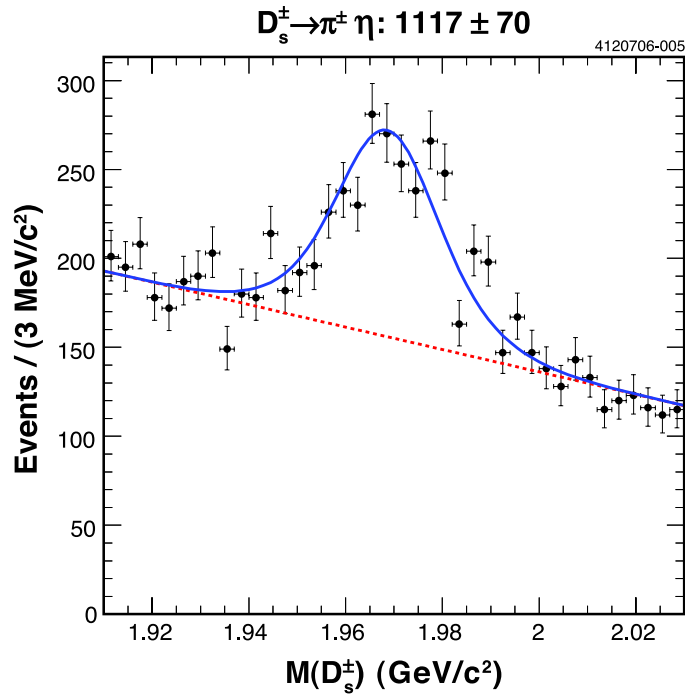


FIG. 6: Fits to single tag data for $D_s^\pm \rightarrow \pi^\pm \eta$.

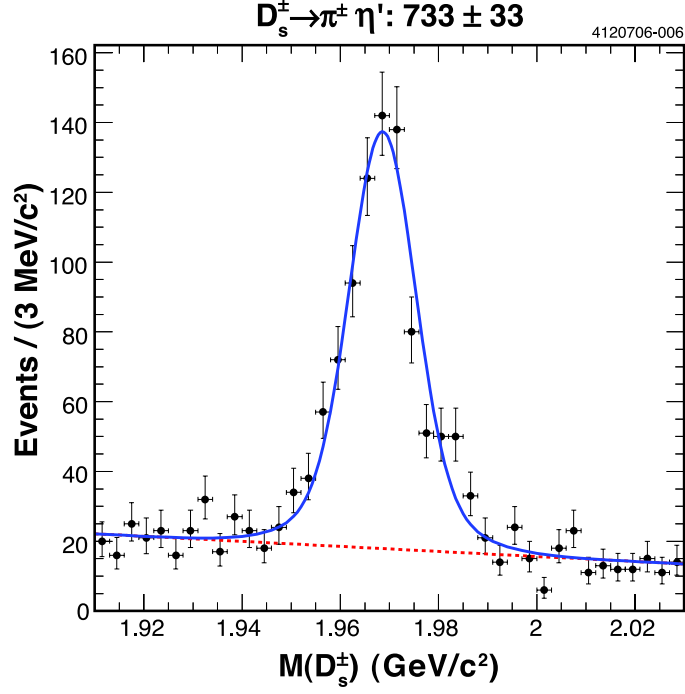


FIG. 7: Fits to single tag data for $D_s^\pm \rightarrow \pi^\pm \eta'$.

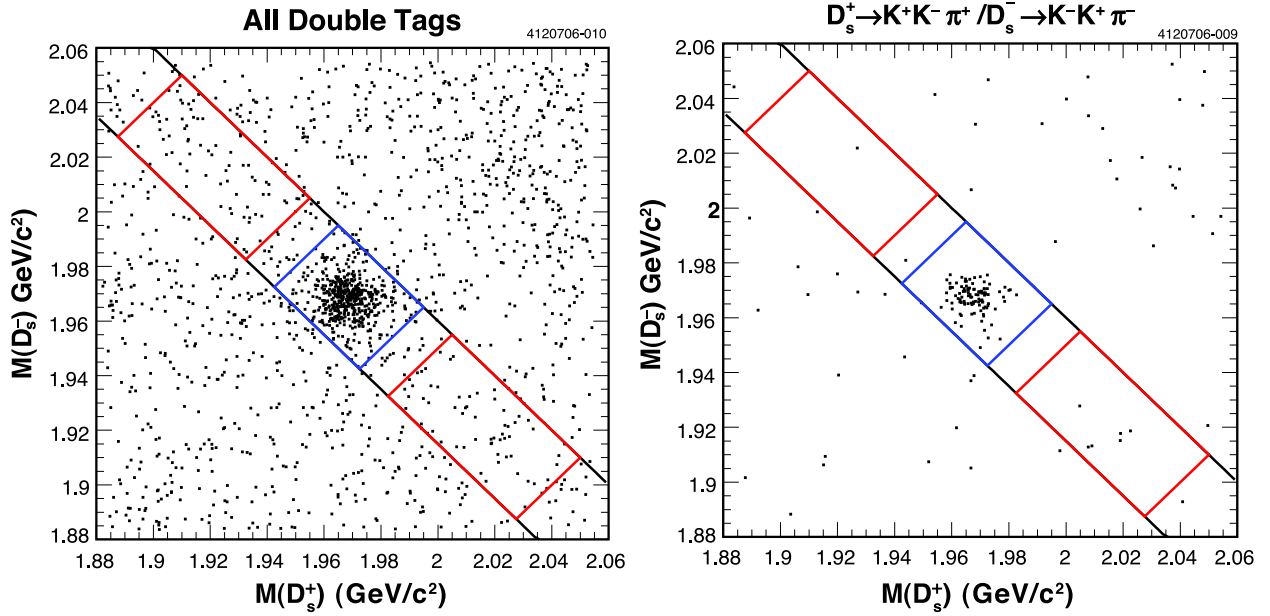


FIG. 8: Scatter plots of $M(D_s^-)$ vs $M(D_s^+)$ for (left) all six D_s decay modes and (right) $D_s^\pm \rightarrow K^- K^+ \pi^\pm$.

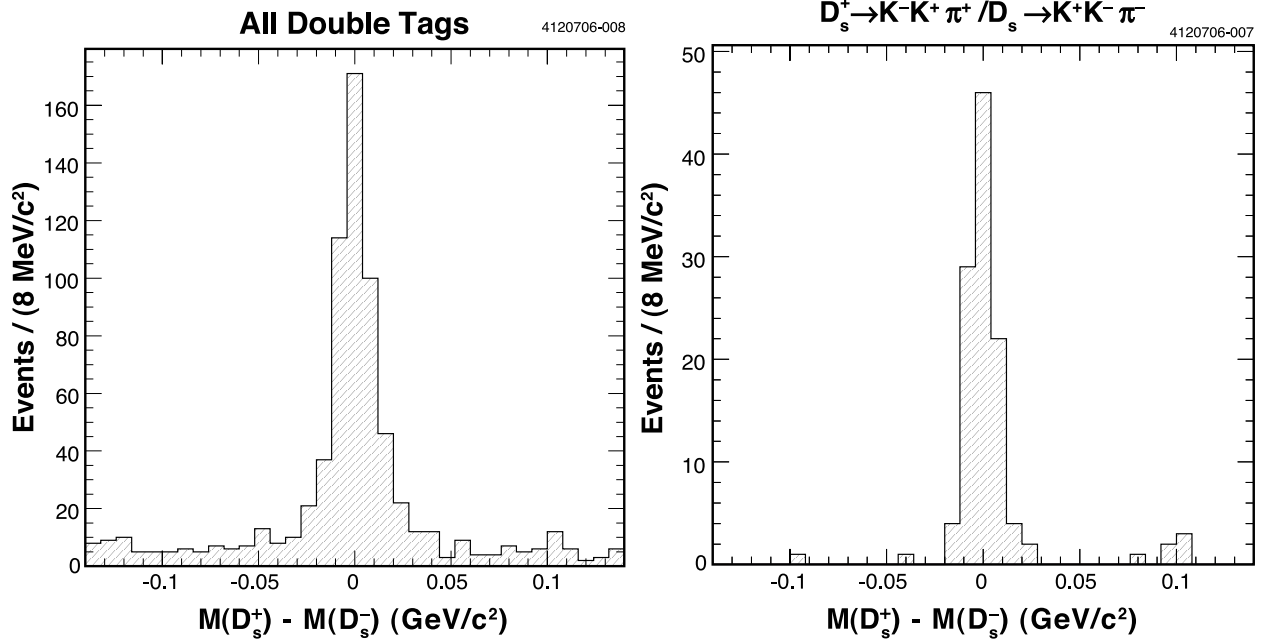


FIG. 9: Projections of $M(D_s^-)$ vs $M(D_s^+)$ scatter plots on the $\Delta M = M(D_s^+) - M(D_s^-)$ axis for (left) all six D_s decay modes and (right) $D_s^\pm \rightarrow K^- K^+ \pi^\pm$.

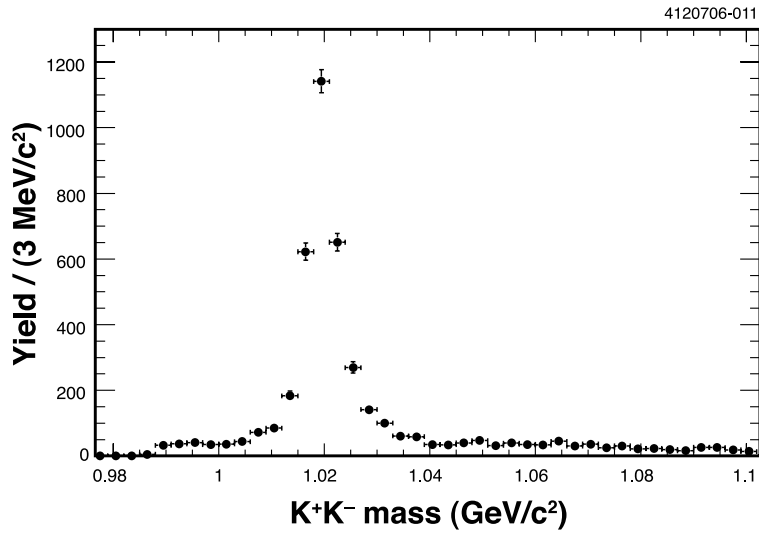


FIG. 10: $M(K^+ K^-)$ distribution for $D_s^+ \rightarrow K^- K^+ \pi^+$ events with $M(K^+ K^-)$ near the mass of the ϕ .

-
- [1] M. Kobayashi and T. Maskawa, *Prog. Theor. Phys.* **49**, 652 (1973).
 - [2] Particle Data Group, S. Eidelman *et al.*, *Phys. Lett. B* **592**, 1 (2004).
 - [3] CLEO Collaboration, M. Artuso *et al.*, *Phys. Lett. B* **378**, 364 (1996).
 - [4] BaBar Collaboration, B Aubert *et al.*, *Phys. Rev. D* **71**, 091104 (2005).
 - [5] MARK III Collaboration, R.M. Baltrusaitis *et al.*, *Phys. Rev. Lett.* **56**, 2140 (1986).
 - [6] MARK III Collaboration, J. Adler *et al.*, *Phys. Rev. Lett.* **60**, 89 (1988).
 - [7] CLEO Collaboration, Q. He *et al.*, *Phys. Rev. Lett.* **95**, 121801 (2005) [hep-ex/0504003].
 - [8] R. Poling, in *Electronic Proceedings of the Flavor Physics and CP Violation Conference, Vancouver, 2006*, (unpublished) [hep-ex/060601].
 - [9] CLEO Collaboration, Y. Kubota *et al.*, *Nucl. Instrum. Methods Phys. Res., Sec. A* **320**, 66 (1992).
 - [10] D. Peterson *et al.*, *Nucl. Instrum. Methods Phys. Res., Sec. A* **478**, 142 (2002).
 - [11] M. Artuso *et al.*, *Nucl. Instrum. Methods Phys. Res., Sec. A* **502**, 91 (2003).
 - [12] CLEO-c/CESR-c Taskforces & CLEO-c Collaboration, Cornell LEPP preprint CLNS 01/1742 (2001).
 - [13] R. Brun *et al.*, GEANT 3.21, CERN Program Library Long Writeup W5013 (unpublished) (1993).
 - [14] D.J. Lange, *Nucl. Instrum. Methods Phys. Res., Sec. A* **462**, 152 (2001).
 - [15] E. Barberio and Z. Was, *Comput. Phys. Commun.* **79**, 291 (1994).
 - [16] CLEO Collaboration, G. Crawford *et al.*, *Nucl. Instrum. Methods Phys. Res., Sec. A* **345**, 429 (1992).
 - [17] Tomasz Skwarnicki, Ph.D. thesis, Institute of Nuclear Physics, Cracow, 1986, DESY Report No. DESY F31-86-02.
 - [18] W.M. Sun, *Nucl. Instrum. Meth. A* **556**, 325 (2006) [arXiv:physics/0503050].
 - [19] E687 Collaboration, P.I. Frabetti *et al.*, *Phys. Lett. B.* **351**, 591 (1995).
 - [20] S. Malvezzi, in *7th Conference on Intersections between Particle and Nuclear Physics (CIPANP 2000)* Quebec City, Quebec Canada, 22-28 May 2000. *AIP Conf. Proc.* **549**, 569 (2002).